

# **DEVELOPMENT OF A CARBON FIBER WHEEL RIM**

Thesis

Presented in Partial Fulfillment of the Requirement for the Graduation with Distinction in the  
Undergraduate School of Engineering at The Ohio State University

By

Aaron Ressa

Undergraduate Program in Mechanical Engineering

The Ohio State University

2013

Thesis Committee

Dr. George Staab, Advisor

Dr. Rebecca Dupaix

Copyright by

Aaron Ressa

2013

## Abstract

In order to improve The Ohio States FSAE student project vehicle performance and improve fuel efficiency, the mass of the vehicle must be reduced. An effective way to do this is to construct the wheels out of a woven carbon fiber composite. In doing so, not only is the overall weight of the vehicle reduced, but rotation inertia and unsprung mass are reduced as well. To do this, physical testing was used to create and validate an FEA model that was then in turn used to develop and analyze a laminated carbon fiber composite rim design. Several designs were evaluated and one was selected for refinement. The final refined design reduced the weight of the wheel by nearly 50%. The wheel was then fabricated and future plans were made to validate and test the wheel so that it may be used on The Ohio States FSAE vehicle during colligate competitions in 2014 competition year.

## Acknowledgements

I would like to thank Dr. Staab for all the time he spent advising me and all the help I've received for various problems with my research and the formula team.

I'd also like to thank the members of the Formula Buckeyes who've spent countless hours helping me, without which this project would not have been possible.

I would also like to thank all the sponsors that contributed to the project as well including Airtech, Henkel, ANSYS, Zyvex, SGS, PPG, and Parker Hannifin.

## Vita

2009 to present.....Mechanical Engineering, The Ohio State University

## Fields of Study

Major Field: Bachelor of Science in Mechanical Engineering

## Table of Contents

Abstract.....	ii
Acknowledgements.....	iii
Vita .....	iv
List of Figures .....	vii
List of Tables .....	viii
1. Introduction and Background .....	1
2. Commercially Available Solutions.....	2
3. Development Process .....	2
4. Material Selection .....	4
5. Material Testing .....	5
6. Packaging Constraints .....	6
7. Loading Scenarios .....	7
7.1 Force Calculations .....	9
8. Experimental Setup and Procedure .....	10
8.1 Experimental Results .....	13

9. Finite Element Model.....	14
9.1 Material Model .....	15
9.2 Finite Element Validation.....	16
10. Design.....	17
10.1 Design Selection .....	20
10.2 Boundary Condition Analysis .....	20
10.3 Initial Design Refinement.....	22
10.4 Localized Reinforcement .....	24
10.5 Final Design .....	25
10.6 Seal Design .....	26
11. Fabrication .....	27
11.1 Layup .....	28
11.2 Fabrication Issues.....	29
11.3 Mold Release Issues.....	31
12. Future Work .....	33
References .....	34

## List of Figures

Figure 1: Comparison of several types of fiber reinforcement's tensile modulus (Staab, 1999) .....	4
Figure 2: Commercial tire dimensions compared to reduced dimensioned tire profile .....	6
Figure 3: View of spindle and brake system assembly inside the rim. ....	7
Figure 4: (Left) Tire Testing rig with pneumatic pistons (Right) Pneumatic control scheme .....	12
Figure 5: Dial Caliper fixed to spindle measuring deflection at the 0 degree orientation on the rim.....	12
Figure 6: lateral deflection vs. the moment applied as a force on tire contact patch.....	14
Figure 7: (Left) Surface used to fix hub face (Right) Remote force applied to tire bead seat faces .....	15
Figure 8: Experimental lateral deflection of the rim compared to FEA results in ANSYS. ....	16
Figure 9: Heighted Faces for reference (Left) Contact Face (Center) Whole contact face (Right) Bolting Contact Face.....	21
Figure 10: Inner and outer deflection as a result of various joining methods.....	22
Figure 11: Comparison of lateral deflection of the inner and outer shells between various layers. ....	23
Figure 12: Contour plot of lateral Deflection of the rim under a cornering load .....	24
Figure 13: Comparison of lateral deflection of the inner and outer shells between initial iterations and reinforcements.....	25
Figure 14: (Left) Revised sealing technique with O-ring. (Right) Original sealing technique with compressed gasket .....	27
Figure 15: Prepreg carbon roll in the process of being cut up for the individual plies.....	29
Figure 16: (Left) First ply of the outer shell placed on the mold (Right) Wrinkling of the joint are plies on the outer shell.....	30
Figure 17: (Left) Inner shell mold being pressed apart (Right) Inner shell part being pressed out of the mold .....	32



## List of Tables

Table 1: Comparison of points earned at competition to improvement required for an 80% average. ....	2
Table 2: Maximum possible G's experience in the lateral and longitudinal direction for each loading case .....	10
Table 3: Forcer based off accelerations for each loading case given a coefficient off friction of 1.5 .....	10
Table 4: Characteristic of the single piece aluminum currently used on the FSAE vehicle.....	18
Table 5: Characteristic of the single piece carbon rim .....	18
Table 6: Characteristic of the single piece carbon rim with bond in spoke section .....	19
Table 7: Characteristic of the two piece rim with aluminum shell and carbon inner shell.....	19
Table 8: Characteristic of the three piece rim, with an aluminum center and carbon shells .....	19

## **1. Introduction and background**

The concept for a light weight wheel arose out of the need for weight reduction in a formula SAE competition vehicle. This vehicle is part of a collegiate race series run by the society of automotive engineers where students design, build, and race a scaled formula style open wheel race car. The wheel was selected for a weight reduction out of the many other components because in addition to a weight reduction, a redesigned wheel rim offers performance benefits as well. The project began with the formula team at The Ohio State University setting a goal to improve an 18<sup>th</sup> place finish at the 2012 Michigan Speedway FSAE competition to a top ten finish. In order to achieve this goal an analysis was done of the competition results, breaking the competition down into its' eight separate events. The past several years of results were analyzed and in order to place in the top ten, it was determined that 800 points out of the 1000 were required. To achieve 800 points, an average of 80% of the points of each event must be earned. This 80% percent threshold was compared to the team's 2012 results and the percent improvement in placing required was calculated in the following table.

**Table 1: Points earned at competition to the improvement required for an 80% average.**

Event	Result	% of Points	Improvement Requirement
Cost	101	22%	32%
Presentation	27	70%	10%
Design	10	67%	13%
Acceleration	42	53%	27%
Skid Pad	25	52%	28%
Autocross	44	53%	27%
Endurance	12	78%	2%
Efficiency	37	22%	58%

Looking at the results it can be seen that the areas that need the most improvement are mostly dynamic events as the highlighted boxes show. For the team to focus on each of the categories individually would be unfeasible. This led to looking at what attributes of the car could be changed and positively affect each of the categories without negatively effecting the others. It was determined that reducing the mass of the car would achieve this goal and provide the most efficient method of improving the cars performance. Furthermore the specific reduction of rotating mass would further increase the car's dynamic abilities all while reducing fuel economy. This conclusion was reached calculations based on the inertia savings in the switch from 13" to 10" tires and an estimated inertial savings based on a wheel weight target of 2.25 lbs. Initial calculations showed that this switch would yield an estimated 4% power increase during acceleration in third gear.

## **2. Commercial Available Products**

Commercially produced 10 inch rims are available from a variety of suppliers. The average weight of the wheels from these suppliers is around 5.1 lbs. This includes a 6061 forged aluminum rim from Keizer racing. Carbon fiber solutions are also available, such as the 2.25 lbs. carbon fiber shell from CS-wheels. The carbon fiber solution excludes the wheel center, which if purchased would bring the whole wheel to about 3.5 pounds. This option only saves one pound from the aluminum solution, and at \$500 per wheel, this solution is prohibitively expensive.

## **3. Development Process**

The design process was broken down into nine different stages. These stages were used to break down the project into manageable mile stones. In addition these steps were also used in synchronizing the development of the wheel rim with the rest of the FSAE vehicle. This interaction with the FSAE team was critical because of the high degree of system integration that happens within the wheel and the dynamic effects it has on the vehicle. The different design phases are as follows:

1. Material Selection
2. Determine Constraints
3. Establish Load Cases
4. Conduct testing on current rim.
5. Setup and validate FEA model with experimental data
6. Develop several different design concepts
7. Select specific design concept and refine design

8. Fabricate the wheel rim
9. Validate the design with physical testing

#### 4. Material Selection

A fiber reinforced plastic was selected as the base material for the rim because they are generally considered to have a high specific strength over many metals. There are several different options for the fiber reinforcement material including glass, carbon, and kevlar. A comparison of the tensile modulus can be seen in the accompanying chart.

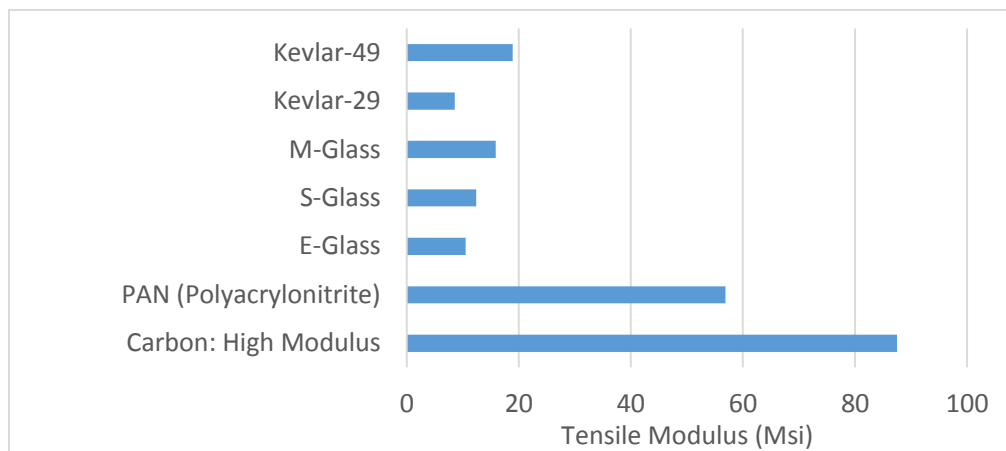


**Figure 1: Comparison of several types of fiber reinforcement's tensile modulus (Staab, 1999)**

Carbon fiber was eventually chosen over glass and Kevlar, not only for its high specific strength, but because of the significant previous experience in the design and fabrication of carbon fiber components as well as the resources available to produce it.

Another consideration when selecting the material is the weave. The weave of the fabric influences the strength of the fabric in the different directions. The main directions of the fabric that are most commonly referenced when describing the strength are the wrap and fill, or the 1

and 2 direction. The wrap fibers run along the length of the fabric and is considered the primary, or 0 degree direction. The fill runs parallel with the width of the fabrics and is considered the secondary or 90 degree direction. Generally carbon fiber is commercially available in three different formats: unidirectional, woven, and braided sleeves. For this project a woven fabric will be used. Braided sleeve was ruled out due to the specialty item cost of such a large diameter, as well as the difficulty in keeping the weave aligned while pulling the sock over the mold. Unidirectional was also ruled out due to the difficulty of handling the fabric during fabrication. A balance between commercial availability and handling during fabrication was found in a 3k twill. The specific fabric selected also was a Zyvex® Arovex prepreg, meaning it comes pre impregnated with resin that allows for a better resin consistency and work time than that of a dry fabric. The Arovex also has the additional feature of having its' resin reinforced with carbon nana tubes, which Zyvex® claims gives a 30% increase in toughness and increased resistance to fatigue. This is ideal in a wheel rim application.

## **5. Material Testing**

An attempt at characterizing the selected carbon was made. Twenty 8 inch by 2 inch samples were laid up at various orientations and number of plies. These samples each had a strain gauge rosette attached at the center of the sample. Each sample was then placed into a pair of self-tightening and aligning clamps. These clamps were fixed to an instron and each sample was pulled in tension at a rate of .003" inches per second. The results of the testing were unsuccessful in determining the elastic modulus of the carbon in the primary and secondary directions. The modulus calculated from the strain gauges varied nearly 50 percent from 7.1 msi to 14.3 msi. However the failure strength did average around 145 ksi. Comparing the

experimental failure strength to the value listed in the material data sheet, the experimentally determined strength was 12 ksi higher than the listed, 133 ksi failure strength. Given that the technical data sheet had listed lower values than the experimental results, it was deemed ok to use the elastic modulus listed in the technical data sheet in the material model to be used in the finite element analysis.

## 6. Physical Packaging Constrains

The wheel shape was determined in the early stages of the design project. This was done to enable the design of the spindle and suspension packing to happen concurrently with the design of the wheel rim. The first step in designing the wheel shape was to determine the correct tire profile for the tire. The industry standard tire profile for a 10 inch tire rim was obtained from the Tire and Rim Association (TRA). The specifications given by TRA and included several features that were not necessary such as retaining hump and a tire mounting groove. These features were removed, which greatly simplified the wheel reducing the number of dimensions needed to constrain the tire profile from 21 to 8, as shown in the figure below.

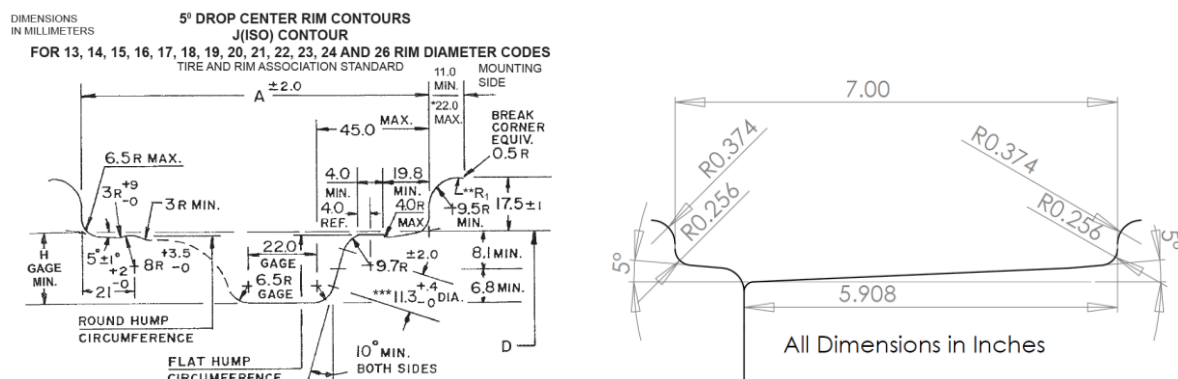


**Figure 2: Commercial tire dimensions compared to reduced dimensioned for the Hoosier**

**RB25C race tire**

The rim offset was determined by the desired track width set by the suspension team. Using the basic profile a general keep out area around the spindle was established. This enabled the suspension design to move forward. Figure 3 shows the wheel shape being test fitted with a proposed upright assembly. This process was done often through the design process to eliminate any possible interference issues.

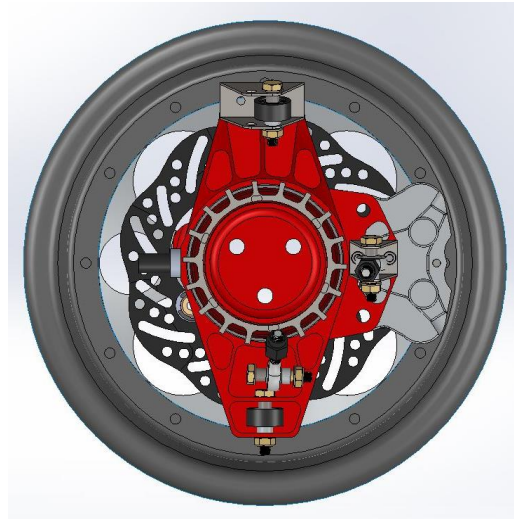


**Figure 3: View of spindle and brake system assembly inside the rim.**

## **7. Loading Conditions**

In order insure the wheel would not fail, four critical load cases where developed to represent the most extreme conditions the wheel rim would experience during operational use. The load cases examined excluded cases examined in commercial consumer vehicle development such as striking a curb or hitting a pothole since the surfaces that the FSAE vehicle runs on is very well known. A detailed description for each load cases used in the analysis are as follows.

- 1) **Cornering Load** – This is the most performance critical of the loading cases as well as the most extensively examined. Not only are the forces on the rim the largest in this case;



the deflection as a result of cornering forces has a significant effect of on the tires performance, and in turn the overall cornering ability of the car.

- 2) The second Load case is acceleration and breaking; the loading of which is the same between the two. The design goal in this case is to minimize the fore and aft rotation of the wheel under acceleration and breaking loads, or what is known as toe change.
- 3) The third load case is the pressurization of the wheel. This case is intended to simulate the tire being over inflated in order to seat the tire bead of the rim. Since the wheel is deflated prior to use, there is no performance concerns during this load case. The only requirement of this case is to insure the wheel rim does not fail during this process. The maximum pressure was determined by the maximum pressure the tire is rated for during the beading process, which for the hosier compound R25B is 40 psi.
- 4) Cornering with acceleration or breaking – This is the most failure critical of the cases examined since the rim in this case will experience the most force. Since breaking and accelerating at a full g-load in a turn would cause the car to lose control, performance in this case is neglected and a purely failure prevention approach was taken. In addition, since large deflections are expected in this case, caliper clearance was also considered, with a minimum of .25” clearance between the wheel and caliper after deflection deemed to be acceptable.

## 7.1 Force Calculations

In order to calculate the load in each case an excel spreadsheet calculator was developed based on the following load transfer equations.

$$\frac{\Delta W_F}{A_y} = \frac{W_s}{t_F} \left[ \frac{H * K_F}{K_F + K_R} + \frac{b}{l} * Z_{RF} \right]$$

$$\frac{\Delta W_R}{A_y} = \frac{W_s}{t_R} \left[ \frac{H * K_R}{K_F + K_R} + \frac{a}{l} * Z_{RR} \right]$$

where,

$W_s = \text{Vehicle Weight}$

$t_F, t_R = \text{Front and Rear Track Width}$

$H = \text{CG Height}$

$K_R, K_F = \text{Front and Rear roll stiffness}$

$a, b = \text{Front and Rear Distance from CG}$

$l = \text{Wheel base Length}$

$Z_{RR}, Z_{RF} = \text{Front and Rear Roll Center Height}$

These equations give the load transfer laterally and longitudinally based on the location of the center of gravity, as well as the roll stiffness of the vehicles when given the longitude and lateral acceleration. From tire data, the maximum possible acceleration in any given direction of the tire is 1.5 g's. Assuming that the maximum coefficient of friction the tire would ever see would be 1.5, the following loads for the given accelerations were calculated.

**Table 2: Maximum possible G's experience in the lateral and longitudinal direction for each dynamic loading case**

Loading Case	Max Possible G Load	
	Lateral	Longitudinal
Cornering	1.5	0
Acceleration	0	1.5
Cornering and Acceleration	1.065	1.065

**Table 3: Forces for each loading case given a coefficient off friction of 1.5**

Forces for Rear Inside Wheel in Pounds				
Force Direction	Cornering	Acceleration	Cornering and Acceleration	Bump
Longitudinal	0	323.25	415.95	0
Lateral	395.85	0	415.95	0
Normal	263.9	215.5	277.3	500

## 8. Experimental Testing

In order to validate the finite element model, a physical testing apparatus was developed. In order to realistically load the rim, the rim needed to be loaded by a mounted tire. The loading of the tire itself was done through the tire contact patch, the area of the tire in contact with the ground.

In industry development of wheel rims, a mounted tire is loaded through the tire contact patch by a rolling sandpaper road. The hub of the wheel is connected to a spindle on a robotic arm that can then apply rotation in the various directions to simulate the loading of the wheel. The

use or construction of such a testing fixture is prohibitively expensive, so a rotationally static testing fixture was constructed for use in this research.

The static test fixture consists of a 3 by 8 inch steel plate, the size of the tire contact patch, which was machined with 24 10-32 threaded holes in it. 10-32 bolts were then grinded down to have a point on them and screwed into the plate so that only the point protruded from the hole.

In order to simulate the different load cases, three 4" diameter parker Hannifin pneumatic pistons were used to apply force in the longitudinal, lateral, and normal directions of the wheel. The lateral and longitudinal pistons were connected to the steel plate with threaded adapters from the piston rods to threaded holes machined into the side of the plate. The normal force was applied to the steel plate by an aluminum cap on top of the piston rod and was lubricated with grease. This allowed movement in the lateral and longitudinal directions without putting side loads on any of the pistons and prevents the pistons from constraining the motion of the tire.

The wheel itself is attached to a steel spindle that incorporates a steel backing plate to simulate the brake hat. The wheel is compressed onto the spindle brake hat by a center lug nut that is torqued to 200 foot pounds as it would be on the actual vehicle.

The control of the pistons was done through three 3-position valves and 3 dial indicated pressure regulators. The force was controlled by knowing the piston diameter and calculating the required pressure. An additional pressure regulator was used in conjunction with a Schrader valve to keep the tire at a constant operating pressure of 12 psi to compensate for

any leaks. The electronic valves themselves were controlled with 3 position switches supplied by a single 24 volt power source. A schematic of the setup is seen in the following figure.

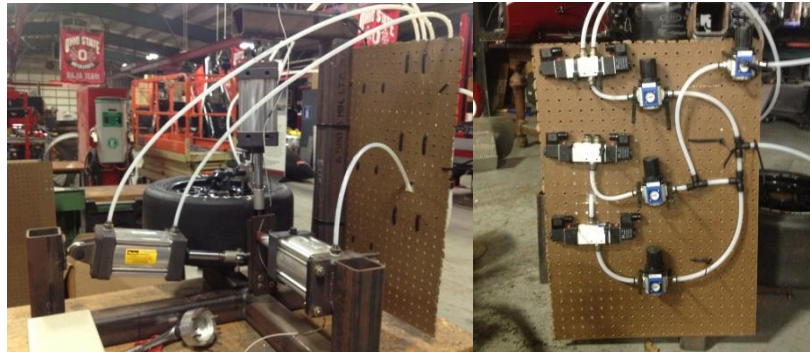


**Figure 4: (Left) Tire Testing rig with pneumatic pistons (Right) Pneumatic control scheme**

The deflection measurements were accomplished using a dial indicator with the base mounted to the top of the spindle. The dial indicator tip was then placed on different points around the wheel to measure the various deflections. Mounting the dial indicator this way was done to eliminate the need to account for any compliance of the testing rig by only measuring the deflection of the wheel rim relative to the spindle.



**Figure 5: Dial Caliper fixed to spindle measuring deflection at the 0 degree orientation on the rim.**

## 8.1 Experimental Results

During the initial assembly of the tire tester it was discovered that drive pins used to constrain the rotation of the wheel on the spindle were not the correct bolt patterns and had to be removed in order to attach the wheel to the spindle. This prevented any longitudinal testing of the wheel and as a result only lateral testing; representing the cornering load case.

Testing was conducted by starting the normal force piston at 15 psi and incrementing in 5 psi increments. The lateral force piston was set to 1.5 times the normal force, representing the force generated by a tire with the theoretical maximum coefficient of friction of 1.5. Each data point was taken by increasing the normal piston force to the desired level and then turning the piston on. The pressure regulator was then adjusted on the lateral piston, toggling the piston off and on till the pressure regulator reached a constant pressure level. Both pistons were then turned off and the dial indicator was read. The normal piston and then lateral piston were turned on and the deflection was recorded. The lateral deflection was tested in both the positive and negative directions.

The moment was calculated by assuming the pistons act at the center of the tire contact patch resulting in a moment due to the normal and lateral forces. The angle of deflection was calculated by taking the tangent of the deflection over the radius of the rim. This method makes the assumption that wheel deforms with a constant slope along the radius, acting as a rigid plate. While this does not capture the true deformation of the wheel, it simplifies the quantization of the wheel deformation for easy comparison.

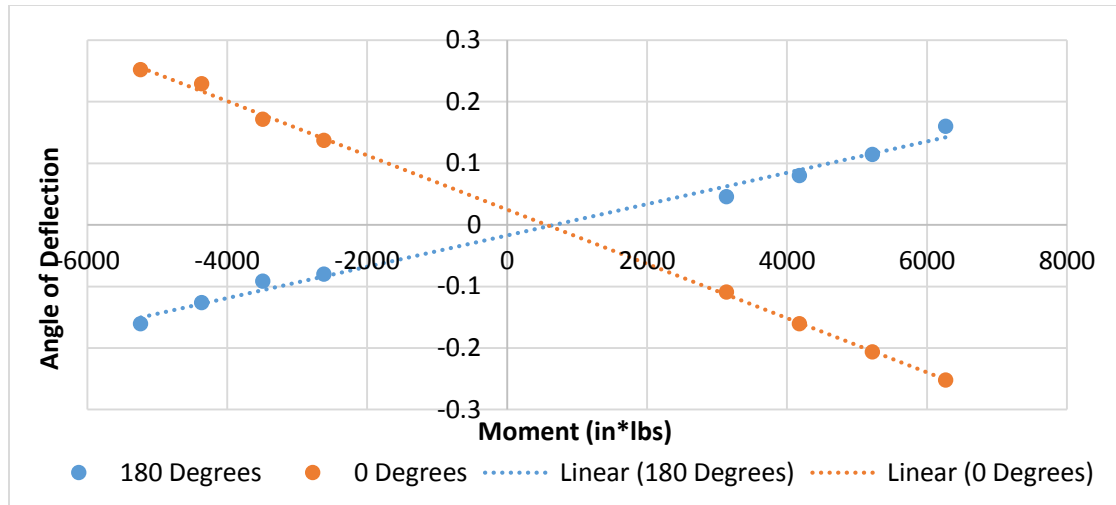


**Figure 6: Plot comparing angle of lateral deflection vs. the moment applied as a force on tire contact patch**

The rim was tested past the maximum cornering load of 4000 in-lbs. to about 6200 in-lbs., the maximum achievable on the test rig. This was done to expand the data set for analysis as well as see if the plastic region of the wheel could be reached. The testing results showed a linear relationship between the moment and the angle of deflection in both the positive and negative moment directions. This indicated the deformations were still in the linear region. At the maximum cornering load the rim deformed approximately .08 degrees.

## 9. Finite Element Model

The structural analysis of the wheel was done with a commercial available finite element solver ANSYS®, utilizing the Composite PrePost® add in package. The package was developed specifically for laminate composites, allowing for easy manipulation of plies and orientations. In addition the package incorporates specific laminate failure theories and analysis methods.

The inner and outer carbon shell was modeled using quadrilateral shell elements, specifically using ANSYS element type, Shell 181. The Aluminum center was model out of solid elements.

### 9.1 Material Model

The rim is normally loaded through the tire. The tire itself is loaded specifically in an area called the tire contact patch, where the tire makes contact with the ground. The tire contact patch size varies for each tire, but from pictures of the vehicle during operation, the tire contact patch is approximately 3 inches by the width of the tire. To simply the loading for analysis purposes, the loading of the tire was considered to be a remote point force at the center of the tire contact patch. This remote force was applied to the rim via the tire bead seat on both the inner and outer sides. The hub face of the rim, which is the section that is compressed against the spindle, was considered fixed. The loading conditions are illustrated in the figure 7.

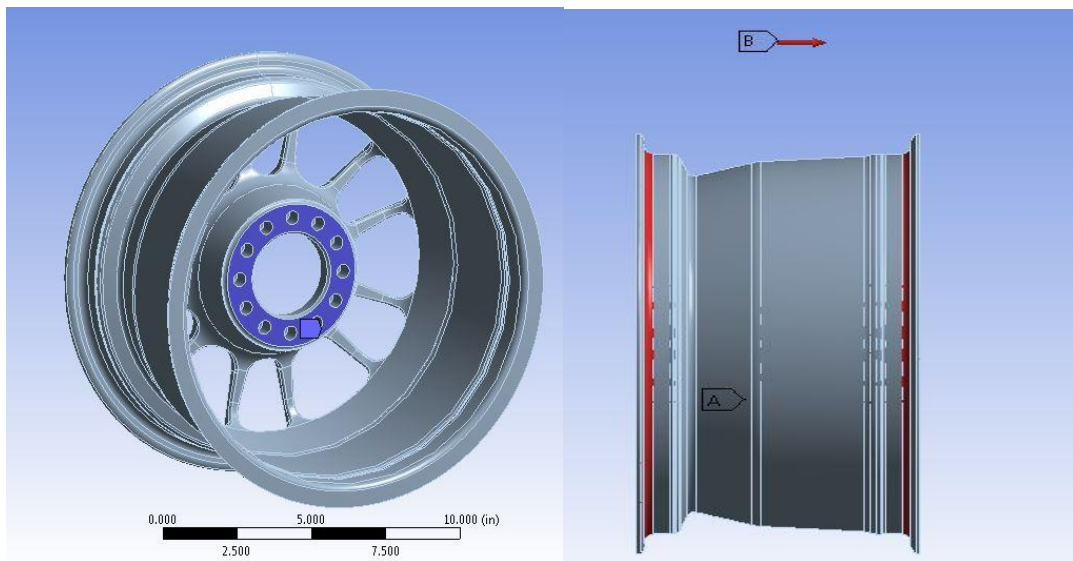


**Figure 7: (Left) Surface used to fix hub face (Right) Remote force applied to tire bead seat faces**



## 9.2 Finite Element Validation

Given that a lot of assumptions were made in the loading conditions, verification of the model was done utilizing the tire testing rig. To do this a model of the wheel was created off drawings supplied by the manufacture. The material used for the model was the ANSYS supplied aluminum alloy model because the manufacture of the rim would not supply the exact alloy of aluminum used for the rim. An analysis was run at each of the experimentally tested data points. The results of the theoretical analysis are overlaid on the experimental results in figure 8.

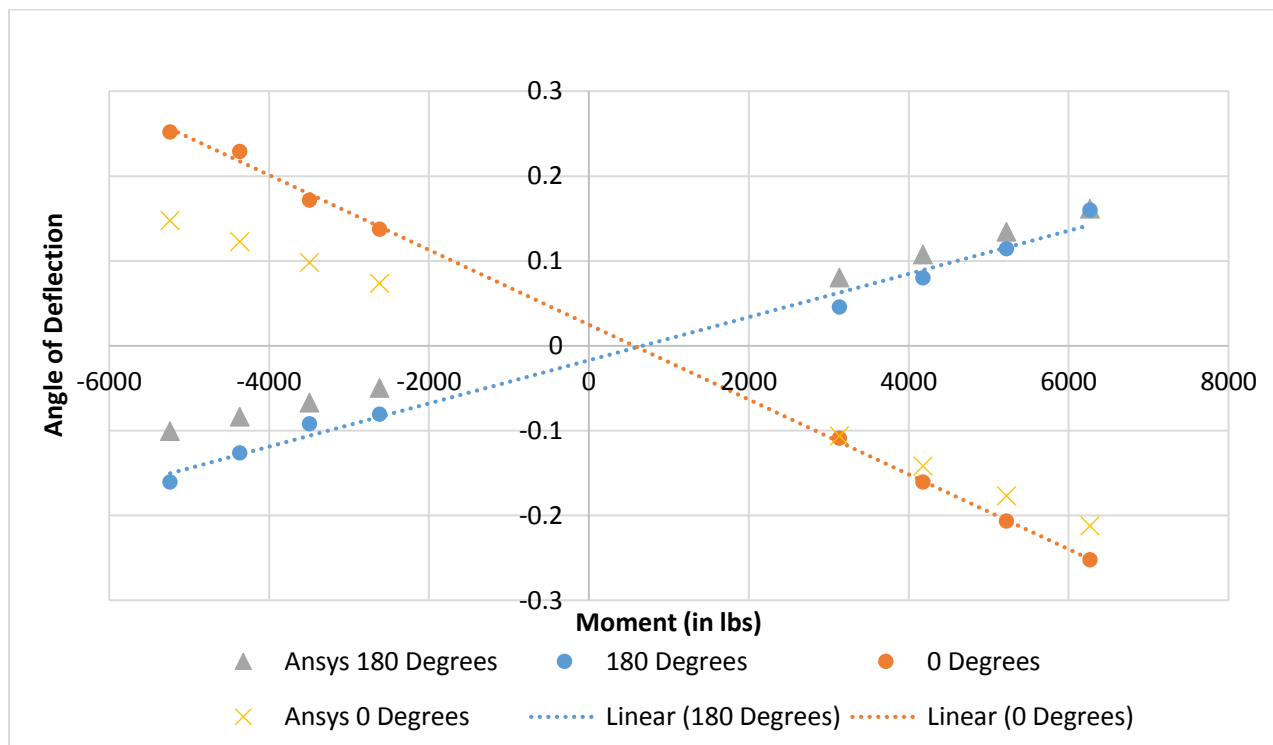


**Figure 8: Experimental lateral deflection of the rim compared to finite element analysis results generated in ANSYS.**

The results show good correlation between the experimental and theoretical results. When a positive moment is applied to the wheel the deflection angle difference is at most .03 degrees, or 13.6%. When a negative moment is applied to the wheel the results differs significantly. The difference between the experimental and theoretical reaches nearly .1 degrees, a 66% difference. While the negative moment results produce an unacceptable amount of error, the rim does not actually see these forces during normal operation. A negative moment is only generated on the inside wheel during coring. This is when the wheel sees the least amount of forces because of the decreased normal force due to the vehicle roll. As a results the negative moment would not present the critical loading case of the wheel. Using this logic it was assumed that the negative moment cases could be ignored. The close correlation of the positive moment results lead to the conclusion that the model was accurate enough to use as the basis of the design analysis.

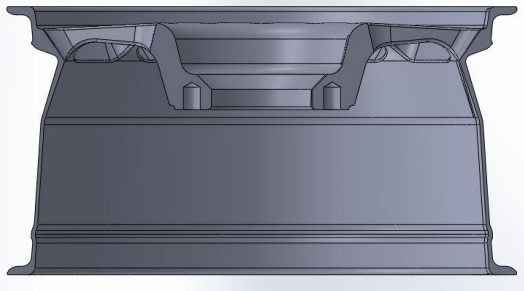
## 10. Design

Once the loading conditions were finalized, five concept designs were developed. In order to compare theses designs without expending a large amount of time refining each design to every loading condition, a specific stiffness metric was developed. This metric was used to evaluate the efficiency of each design compared to the weight of it. It was calculated per the following equation:


$$\text{Specific Stiffness} = \frac{\frac{\text{Applied Moment (in * lbs)}}{\text{Deflection (Lateral Degrees)}}}{\text{Wheel Weight (lbs.)}}$$

The five different concepts are shown in the tables below with the accompanying specific stiffness.

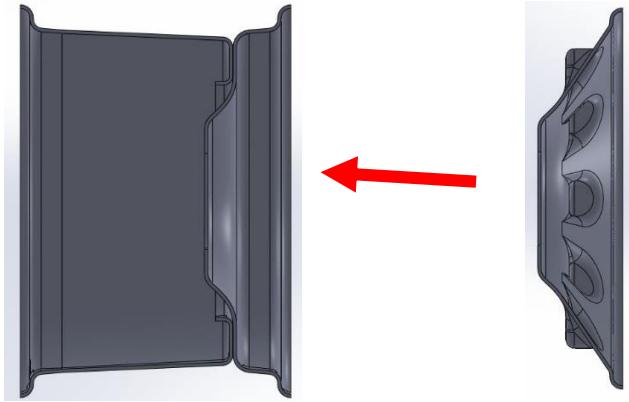
**Table 4: Calculated characteristic of the single piece aluminum currently used on the FSAE vehicle**

	Moment (in*lbs.)	3900
	Weight (lbs.)	7.1
	Deflection Angle (Degrees)	0.036
	Stiffness (in*lbs./Degrees)	84782.6
	Specific Stiffness (stiffness/lbs.)	11941.2
	Description: This is the original OZ-13 single lug, solid aluminum wheel purchased from OZ.	


**Table 5: Calculated characteristic of the single piece carbon rim**

	Moment (in*lbs.)	3900
	Weight (lbs.)	1.73
	Deflection Angle (Degrees)	.21
	Stiffness (in*lbs./Degrees)	18571.4
	Specific Stiffness (stiffness/lbs.)	10734.9
	Description: A single piece rim that is made of carbon fiber. The rim 8 plies overall, with 6 additional reinforcements added to the hub.	


**Table 6: Calculated characteristic of the single piece carbon rim with bond in spoke section**

	Moment (in*lbs.)	3900
	Weight (lbs.)	1.97
	Deflection Angle (Degrees)	.14
	Stiffness (in*lbs./Degrees)	27857.1
	Specific Stiffness (stiffness/lbs.)	14140.7
	Description: This design is similar to the single piece carbon rim but has a bonded in spoke plate that creates a straight load path from the tire bead seat to the hub.	

**Table 7: Calculated characteristic of the two piece rim, with aluminum outer shell and carbon inner shell**

	Moment (in*lbs.)	3900
	Weight (lbs.)	3
	Deflection Angle (Degrees)	.275
	Stiffness (in*lbs./Degrees)	14181.8
	Specific Stiffness (stiffness/lbs.)	4727.27
	Description: This 2 piece design consists of an outer and hub section made out of 7575 aluminum with an inner shell made of carbon fiber.	

**Table 8: Calculated characteristic of the three piece rim, with an aluminum center and inner and outer carbon shells**

	Moment (in*lbs.)	3900
	Weight (lbs.)	1.983
	Deflection Angle (Degrees)	.28
	Stiffness (in*lbs./Degrees)	13928.6
	Specific Stiffness (stiffness/lbs.)	7023.99
	Description: This is a three piece design with a separate carbon inner and outer shell. The center is a separate 7075 aluminum piece.	

## **10.1 Design Selection**

Of the five designs compared, the single piece-bond in spoke had the heights specific stiffness. While the specific stiffness compared the relative strength of the designs, other factors had to be considered. The development up to this point in the design process had been delayed, in turn, design fabrication design became the dominate constraint. The fabrication of both a single piece wheel with the addition of the bond in spoke became prohibitive. Once this design was ruled out, the single piece carbon wheel and the three piece with carbon shells became the leading designs. While the single piece had a higher specific strength, it was not a significant enough increase when considering the tire changing producer of the three piece compared to the single piece. The single piece requires a professional tire mounter, whereas the three piece can be done in house, and on the track. Given these considerations the three piece with carbon shells and an aluminum center was selected for refinement.

## **10.2 Boundary condition analysis**

Before the initial design began an analysis was conducted to take a look at the boundary conditions concerning the joint of the three piece wheel since it was not considered in the FEA model validation with the single piece wheel on the tire tester. In order to do a comparison of several different joining methods, three regions on the joint faces were defined in figure 9.

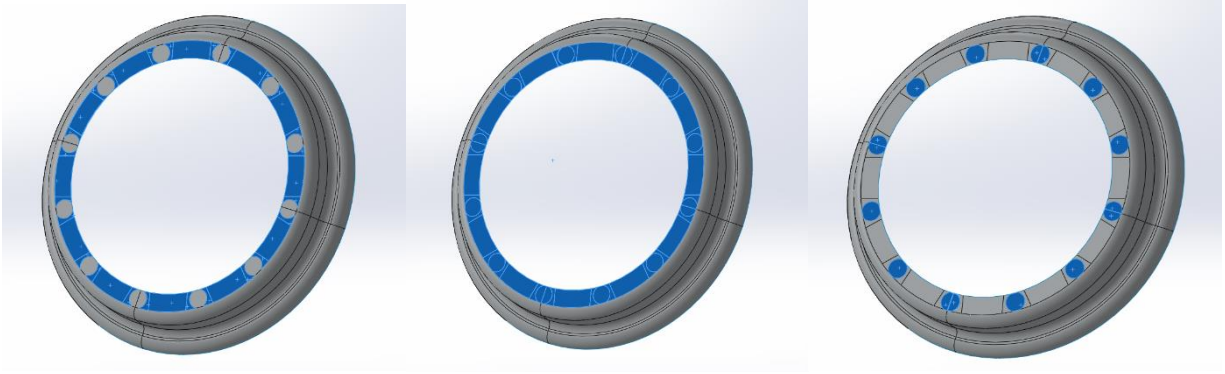


**Figure 9: Heighted Faces for reference (Left) Contact Face (Center) Whole contact face (Right)**

### **Bolting Contact Face**

Four different joint methods were used. The first, and most realistic condition, bonded the bolt area and created a no penetration condition for the contact face. The second bonded the bolt area and had a no separation condition for the contact face. The third bonded the whole face while the fourth bonded just the bolting area. From the results, shown in figure 10, the first and fourth condition show similar results, but while the fourth setup takes 6 minutes to run a complete simulation, the first joint methods takes 128 minutes. As a results, while the first condition is the most realistic, the fourth method presents the most efficient method when considering the time constraints of the project.

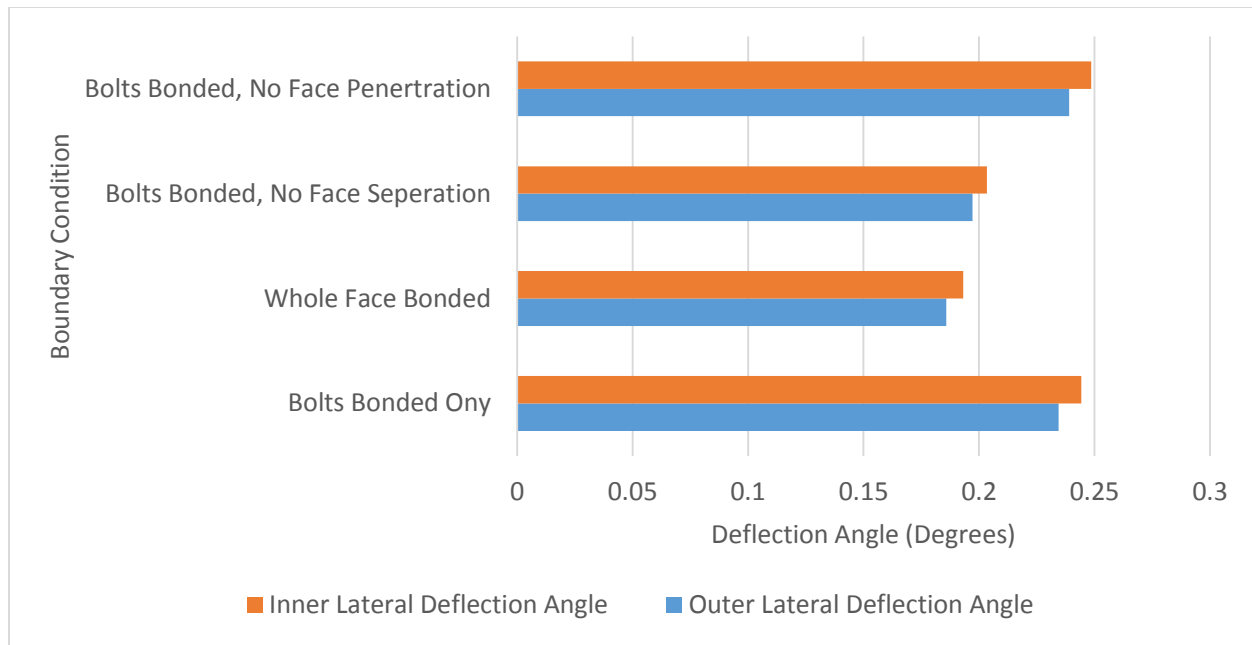


**Figure 10: Inner and outer deflection as a result of various joining methods of the three piece wheel**

### 10.3 Initial Design refinement

The initial design began with developing the fabrication method in terms of the best ply shapes that work with the wheel mold. Based on draping experience from fabrication of previous carbon fiber parts it was determined that most consistent ply shapes would be circular patterns, with a single rectangular pattern for the large hoop section on the inner shell. These shapes were chosen over another method of using 4-5 inch strips the lay across the width of the wheel because it eliminates the overlap between the strips. This is important because the overlap could introduce inconsistencies in the wheel layup that could in turn unbalance the rim, requiring the use of wheel weights. It also doesn't all for continuous fibers around the circumference of the wheel which thereby weaken the wheel. Next a basic orientation scheme was developed, where the orientation of layers alternate between the 0 and 45 degree

orientation. This was done to create a stiffness and strength that would not vary too drastically relative to the orientation of the wheel. Additional orientations with finer steps to create a more quasi isotropic material were considered but eventually determined to be too much of a complication during the fabrication process.

Given the pattern and orientation constrains the analysis of the wheel was conducted by iterating the amount of layers over the inner and outer shell. The stiffness was compared to total weight of the wheel, including bolting hardware and the wheel center. The results of this iteration from 10 to 16 layers in increments of 2 plies in comparison to each other as well as the commercial 10" are shown in figure 11.

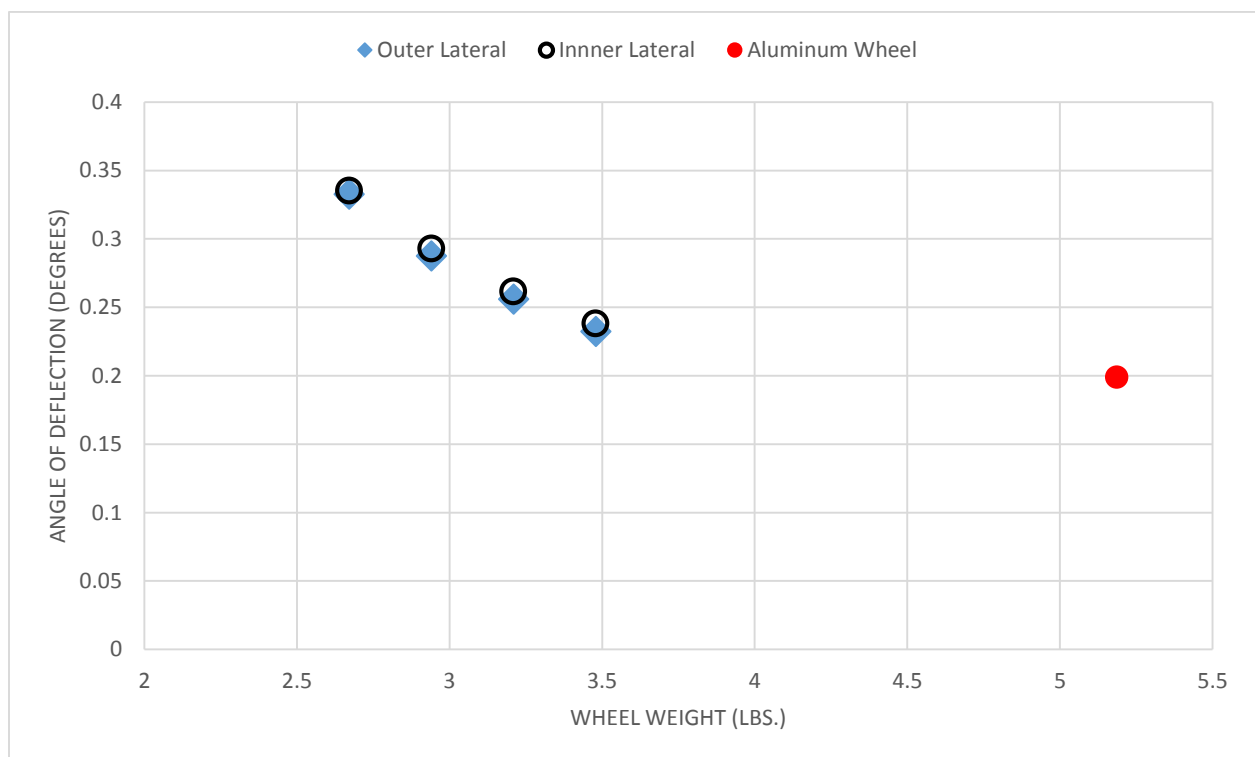


**Figure 11: Comparison of lateral deflection of the inner and outer shells between 10, 12, 14, and 16 layers.**



## 10.4 Localized Reinforcement

Once the target stiffness was approximately reached, a failure analysis was conducted to see if the required strength had been reached as well. Initially a failure analysis was conducted utilizing the max stress criteria, which involves comparing the max principle stresses to the defined max strength of the material in the respective directions. Additionally interactive failure theories were also evaluated including Tsai-hill and Tsai-Wu. From this analysis a factor of safety to was determined to exceed 20 for most of the rim outside the joint area. The lateral deflection was also analyzed. It is seen that the significant majority of deflection occurs at the joint area between the halves of the wheel. Figure 12 illustrates this with a lateral deflection contour plot.

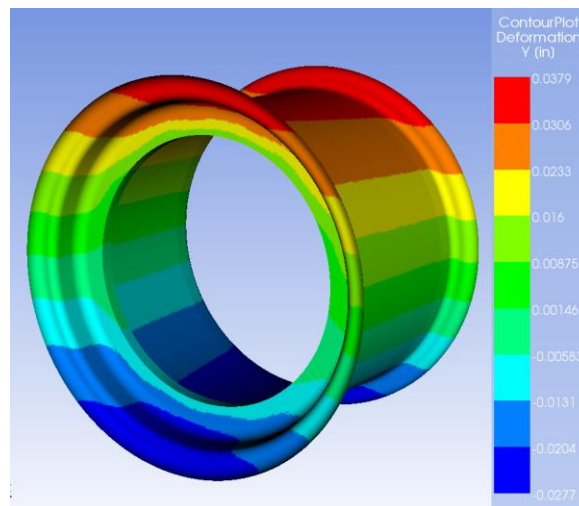


**Figure 12: Contour plot of lateral Deflection of the rim under a cornering load**

Based on the failure and deflection results, the plies in the outer portions of the wheel near the tire bead were reduced while adding reinforcement plies to the joint area of the carbon shells. In addition the orientation of the plies that make up the hoop section of the inner shell was

changed to a 0 degree orientation relative to the circumference of the rim in order to increase the hoop strength. Simulations consisting of variations of both reinforcement plies and number of reduced outer plies showed a similar strength to the original iterations while reducing the weight of the wheel. Figure 13 shows these results overlaid on the initial design iterations, where the new iterations are shown further to the left, with similar strength but a weight reduction of nearly a pound.

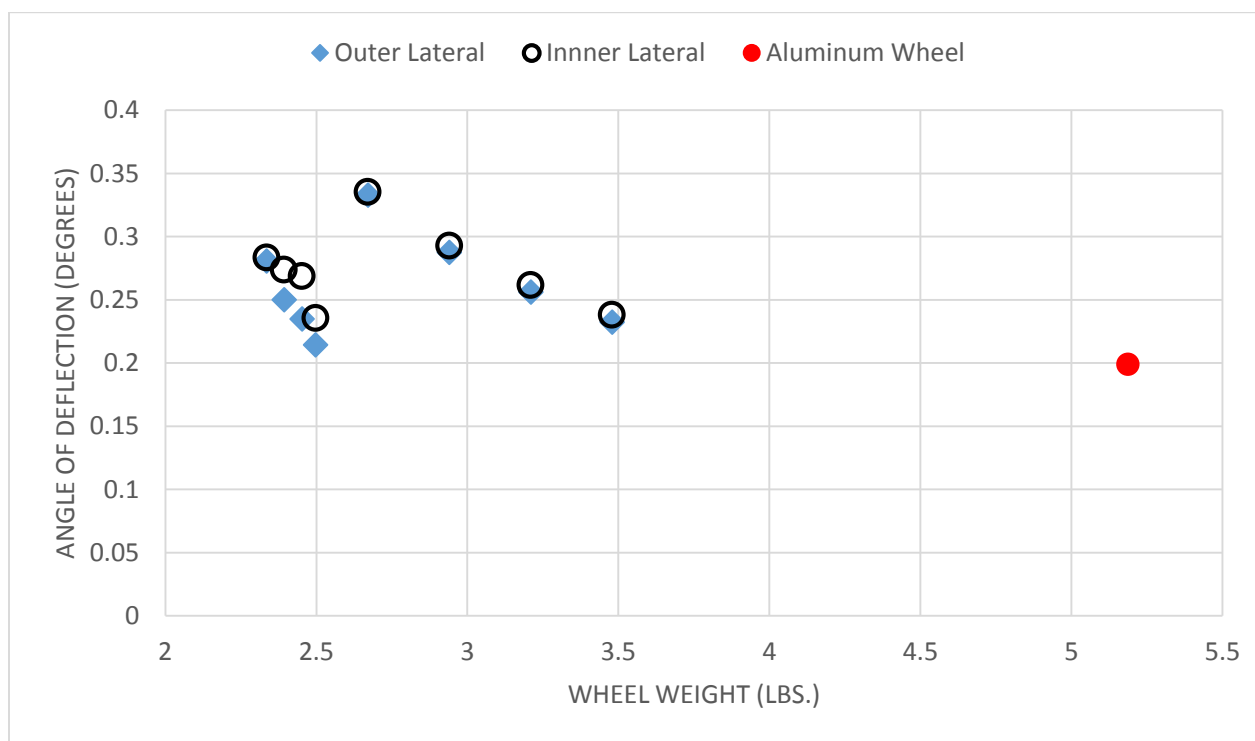


**Figure 13: Comparison of lateral deflection of the inner and outer shells between initial iterations and reinforcements.**

### Final design

The final design was the chosen to be the stiffest design of the reinforcement iterations, with a predicted stiffness within 6% percent of the aluminum wheel. Based on the density of the

carbon and aluminum the inner shell was estimated to be .89 lbs.; the outer shell was estimated to be .46 lbs.; and the center was estimated .823 lbs. The bolting hardware was weight and found to be .35 lbs. in total. This results in a total wheel weight of 2.52 lbs., a 2.6 lbs. savings over the commercial wheel weighing 5.1 lbs.

### **Sealing Design**

Initially the wheel was designed to be sealed by a gasket between the carbon shells and then compressed by bolting the center to outside of the outer carbon shell. Several gaskets were obtained ranging in materials from paper to an assortment of polymers. These were intended to cover the entire sealing face as seen in figure 14. After examining the gaskets it was determined that the polymer gasket would introduce a significant amount of compliance into the wheel. The paper gasket was tested by attempting to seal an old 13 inch three piece wheel. The paper gasket failed to seal the wheel without the use of a silicon sealant. The method of using this sealant to assist the sealing of a three piece wheel had been used in past by the formula team and has failed several times. To increase the reliability of the seal, the sealing interface was redesigned to include an O-ring. In addition the center was reduced in diameter by .75 inches and the inner lip of the carbon shells extended .25 inches to incorporate a seating area for the O-ring.

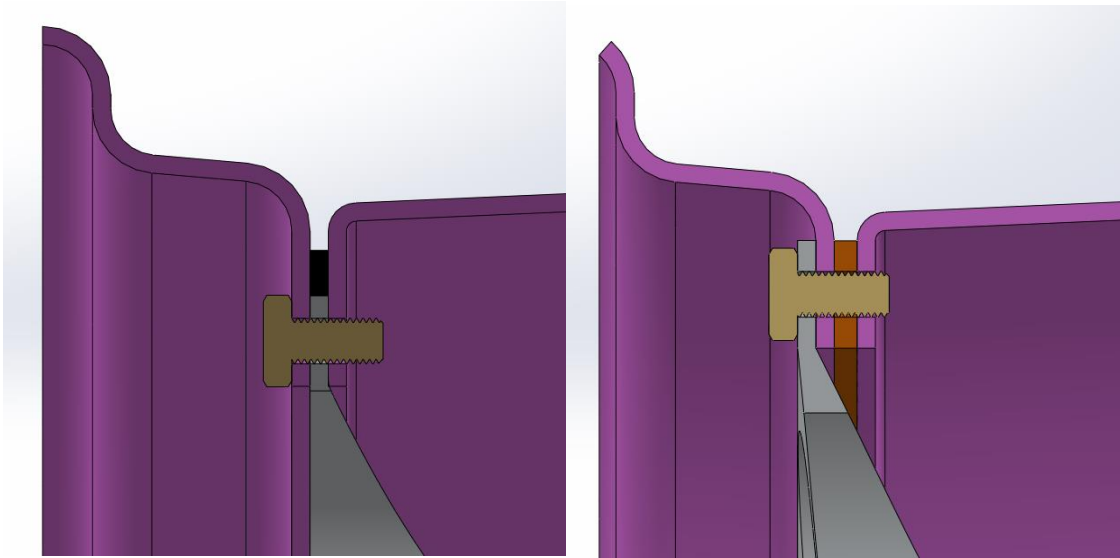


**Figure 14: (Left) Revised sealing technique with O-ring. (Right) Original sealing technique with compressed gasket**

## **11. Fabrication**

The fabrication of the wheel began with the mold. The design of the mold begins with determining which faces of the part are critical and require a mold face to achieve the desired tolerance of the part. The most tolerance critical face of the wheel is the bead seat radius and the draft angle away from the bead seat. To provide a mold face for this face, the wheel mold must be a female mold, meaning that the part is formed inside a mold cavity, as opposed to a male mold, where the part is formed over a mold boss. This method also provides a high quality finish on sealing face.

Typically the formula team uses Renshape 460, a poured plastics, for the mold material in order to reduce cost. This material is not suitable for use with a prepreg material because the curing temperature is higher than the glass transition temperature. The molds instead were constructed out of 6061 aluminum machined using a CNC. The outer shell mold was

constructed out of a single piece of billet. The inner shell mold was made from two separate pieces that vertically stacked and located to each other using four quarter inch pins. The two piece mold also had a .125" groove cut along the perimeter of the top half in order to provide a pry point to separate the two halves. After machining the mold, it was sanded with 400 grit sand paper to eliminate the cusp tool marks. The sanding was then stepped up to 800 grit and then polished.

### **11.1 Layup**

Once the plies were determined in ANSYS, a draping simulation was conducted to determine the flat wrap of each ply area. This process converts 3d plies into 2d patterns that were printed and transferred to card stock. In total 7 unique templates were constructed. These templates were then labeled with their name and number needed of each ply.

The prepreg carbon roll was removed from freezer storage and allowed to set a half hour to become pliable enough to unroll. The carbon plies are then cut out of the carbon sheet using the templates and a box cutter. Once the carbon plies are cut out they are placed back in the freezer. Even though the carbon has a shelf life of 14 days at room temperature, the time at room temperature is minimized to decrease the viscosity the resin, decreasing the chance of voids in the part, and the resin volume fraction.



**Figure 15: Prepreg carbon roll in the process of being cut up for the individual plies.**

The mold is coated with WOLO, a release agent that prevents the resin from bonding with the mold. Several coats are applied to ensure no areas are missed. In addition to the part surface it is important to apply release to all surfaces of the mold including the joint between the mold halves and the pins that locate them. The carbon patterns are then laid into the mold one by one. This results in the patterns interlacing. This increases the total bonding area between the plies decreasing the chance of failure along the ply joints.

### **11.2 Fabrication Issues**

Several issues were encountered laying in the carbon. The resin in the prepreg retained a very high viscosity at room temperature and greatly reduced the ability of the plies to drape over the geometry of the rim. The plies on the tire bead area of the rim were unable to drape over the tire bead seat radius and had to be slit in order to completely adhere to the radius. This was undesirable as the cut fibers interrupted the direct load paths through the fibers. In addition uneven slits over the entire buildup of plies could lead to an unbalanced wheel. The plies

reinforcing the joint area of the wheel also caused issue when contouring to the internal radius, wrinkling at the top of the template. This also led to uneven carbon buildup affecting the balance of the rim.



**Figure 16: (Left) First ply of the outer shell placed on the mold (Right) Wrinkling of the joint are plies on the outer shell.**

The templates are used again to cut p3, a release film. This film is placed over the carbon layer, sticking to the resin and preventing the bleeder cloth from bonding to carbon. Small holes cut in the film allow excess resin to pass through during curing. The p3 is not as pliable as the carbon fabric and must be cut into pieces to allow it to conform to the contour of the wheel mold. Gaps where the slits were made must be covered with additional pieces of p3.

Bleeder cloth is placed over the p3. It consists of loosely woven cotton. The bleeder cloth serves two purposes. First, it acts as a sponge to soak excess resin and small air bubbles out of the part during the curing process. Second, it provides a pathway for the air to travel when vacuum is applied. Without the bleeder cloth, the vacuum bag would be pressed against the mold directly and cut areas farther away from the vacuum off, in turn preventing excess resin and air being

draw from the entire part. The bleeder cloth is secured into place with special high temperature tape. The cloth is only loosely secured, allowing the cloth to move and be drawn into tight radii as the vacuum is applied. This prevents bridging, allowing force of the vacuum bag to reach deep into the radii.

Once bleeder cloth has been placed over the part, the mold is placed into a vacuum bag. A nozzle is added to attach a vacuum line. Vacuum is drawn and the bag is adjusted to remove any bridging and form pleats, which folds of excess vacuum bag. Pleats are used to prevent bridges in the bag from forming as the pressure increases on the part and the carbon layers are forced closer together. The bag is checked for leaks along the tape seams.

The molds are then placed into an autoclave. The autoclave is pressurized to 80 psi while vacuum is still being applied to part. Once the integrity of the seal of the vacuum bags is confirmed by monitoring the pressure of the vacuum system accumulator, the autoclave is heated 250° F at a ramp of 2° F per minute and then heat soaked for 2 hours. Since the autoclave has no cooling system, the pressure is relived at after the heat soak and the part is allowed to naturally cool for about 2 hours till it reaches 150° F. The part is then removed from the autoclave.

### **11.3 Mold Release Issue**

In the autoclave the aluminum mold is heated up to 250 F before the resin starts to cure. As a result the carbon part will cure in the mold's thermally expanded state. As the autoclave cools down the carbon wheel is slowly compressed into the mold as it contracts. Given this fact, once



the part is removed from the autoclave, it is removed from the mold as quick as possible while the aluminum is still hot.

Initially, screw drives and crowbars were used in an attempt to pry the two halves of the outer mold apart along the machined in pry point. This resulted in denting the mold along the pry point and as well as being unable to separate them. Larger .5" tall and .75" deep grooves were machined into the top half of the outer shell mold. These larger grooves allowed angle iron to suspend the mold off the base of a hydraulic press. The press was then used to push on the bottom of the bottom section of the mold separate it from top half. The top mold was then placed in the press upside down. A piece of tooling board was placed across the top of the inner joint area and used to press the carbon rim out of the mold. This required nearly 2000 lbs. of force.



**Figure 17: (Left) Inner shell mold being pressed apart (Right) Inner shell part being pressed out of the mold**

Since the outer shell did not have a point the allowed the carbon shell to be pressed out, a crow bar was used in an attempt to pry the joint area from the mold. The rim cracked before being able to be released from the mold, ruining the part. The outer shell mold was redesigned to be two pieces, with large grooves in the top half, so it could be separated and removed from the mold as the outer shell had been.

## **12. Future Work**

Fabrication delays and issues with the outer shell releasing from the mold have delayed the fabrication of the final wheel to outside the time frame allowed for this research to continue. The wheel construction will continued with plans of being finished by the end of December 2013 with on car testing scheduled to begin in early February 2014. In addition results from the experimental testing are expected to contribute the development of an accurate material model to be used in the development of other carbon fiber parts for the Formula Buckeye team.

## References

Anonymous. (2013). ANSYS Help System version 14.5.7. Canonsburg, PA, USA.

Anonymos\_2 (2013). Arovex Technical Data sheet. North Dakota, USA: Zyvex.

Staab, G. H. (1999). *Laminar Composites*. Woburn: Butterworth-Heinemann.

Chapman, Matthew K. (2011). *Development of a Composite Wheel Rim for an FSAE Car*.

Smith, C. (1984). *Engineer to Win Understanding Race Car Dynamics*. Minneapolis: MIB  
Publishing Company.

Milliken, W. F., & Milliken, D. L. (1995). *Race Car Vehicle Dynamics*. Warren dale: Society of  
Automotive Engineers.